ELECTRONIC SUPPLEMENTARY INFORMATION

Photocatalytic, Structural and Optical Properties of Mixed Anion Solid solutions $Ba_3Sc_{2-x}In_xO_5Cu_2S_2$ and $Ba_3In_2O5Cu_2S_{2-y}Se_y$

Gregory J. Limburn[a], Matthew J. P. Stephens[a], Benjamin A. D. Williamson[b], Antonio Iborra-Torres[a], David O. Scanlon[c], Geoffrey Hyett[a]

[a] School of Chemistry, University of Southampton, Southampton, SO17 1BJ, United Kingdom
[b] Department of Materials Science and Engineering, Norwegian University of Science and Technology (NTNU), Trondheim 7491, Norway
[c] Department of Chemistry, University College London, 20 Gordon Street, London, WC1H 0AJ, UK
[d] Thomas Young Centre, University College London, Gower Street, London WC1E 6BT, United Kingdom
[e] Diamond Light Source Ltd., Diamond House, Harwell Science and Innovation Campus, Didcot, Oxfordshire OX11 0DE, UK
*Corresponding Author: g.hyett@soton.ac.uk

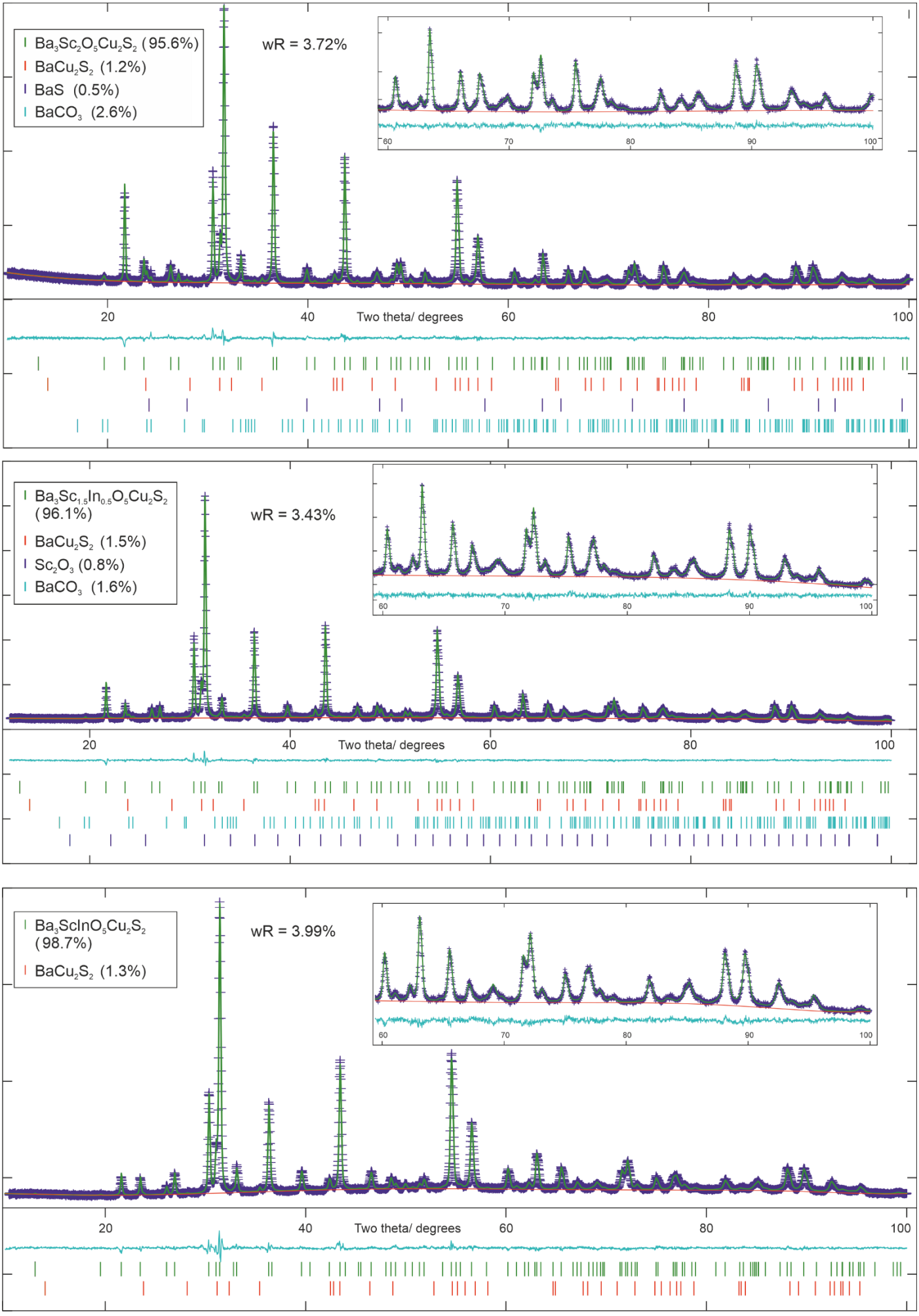

Fig S1. Rietveld refinements of XRD patterns collected on $Ba_3Sc_2O_5Cu_2S_2$, $Ba_3Sc_{1.5}In_{0.5}O_5Cu_2S_2$, and $Ba_3ScInO_5Cu_2S_2$

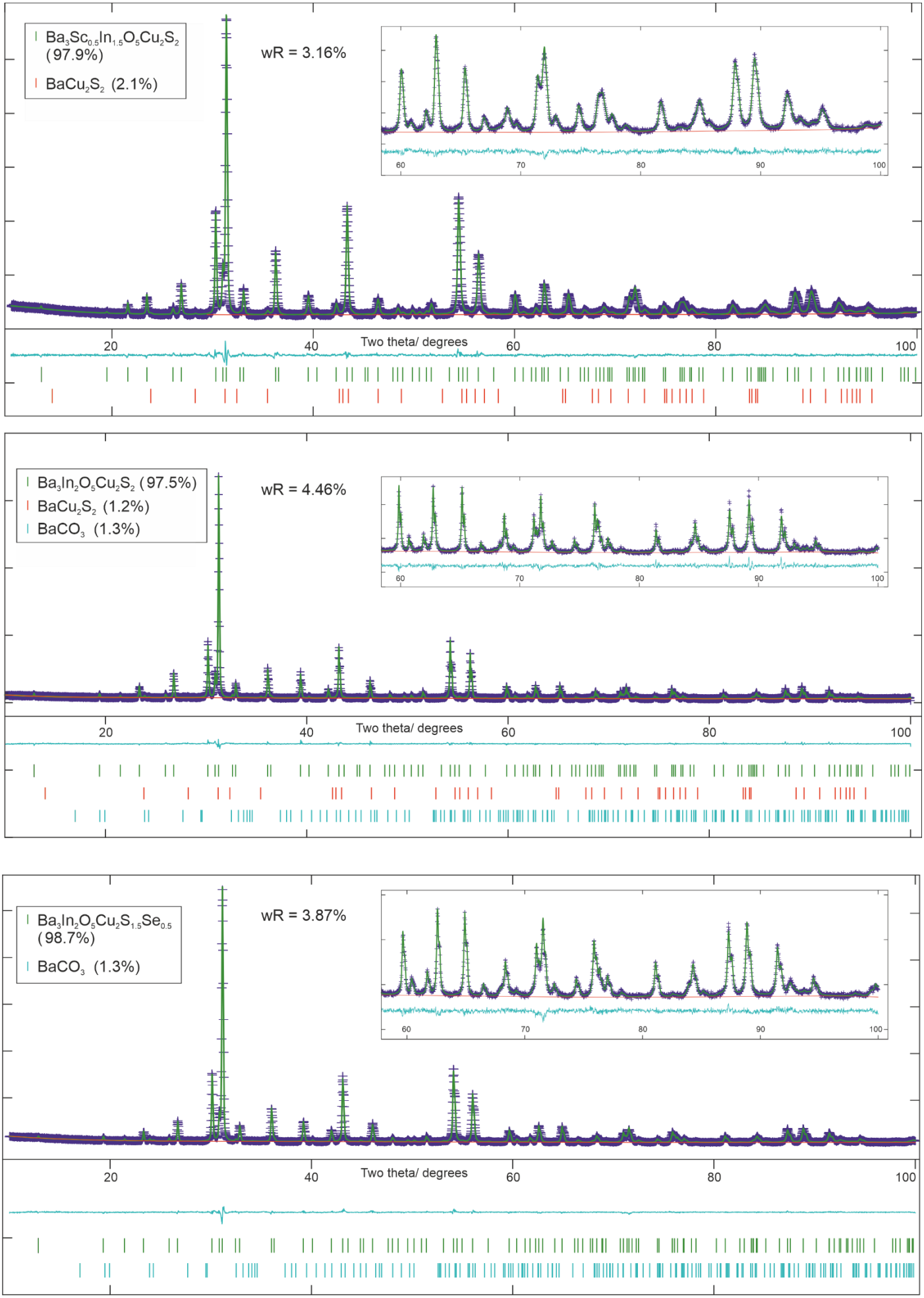

Fig S2. Rietveld refinements of XRD patterns collected on $Ba_3Sc_{0.5}In_{1.5}O_5Cu_2S_2$, $Ba_3In_2O_5Cu_2S_2$, and $Ba_3InO_5Cu_2S_{1.5}Se_{0.5}$

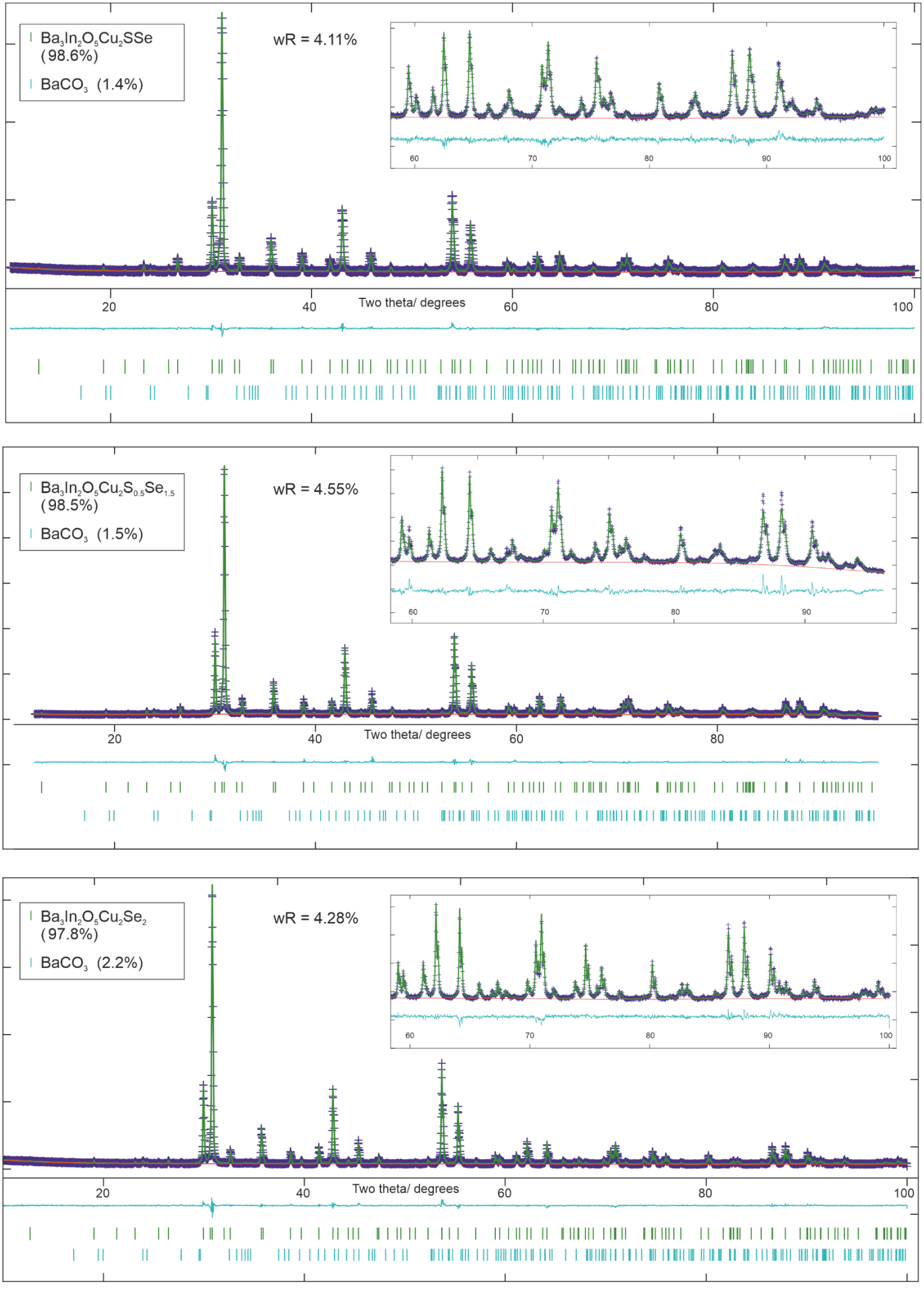

Fig S3. Rietveld refinements of XRD patterns collected on $Ba_3In_2O_5Cu_2SSe$, $Ba_3InO_5Cu_2S_{0.5}Se_{1.5}$, and $Ba_3InO_5Cu_2Se_2$

	$Ba_3Sc_2O_5Cu_2S_2$	$Ba_3Sc_{1.5}In_{0.5}O_5Cu_2S$	$Ba_3ScInO_5Cu_2S_2$	$Ba_3Sc_{0.5}In_{1.5}O_5Cu_2S$	$Ba_3In_2O_5Cu_2S_2$
Lattice parameter a	4.1458(2)	4.1577(2)	4.1680(3)	4.1772(1)	4.1862(1)
Lattice parameter c	27.136(2)	27.218(2)	27.317(4)	27.401(2)	27.444(1)
Cell Volume	466.42(6)	470.50(5)	474.55(8)	478.12(6)	480.95(2)
Data Points	4444	4444	4444	4444	4345
Reflections (325 phase)	100	101	101	102	98
Refined Parameters	33	29	24	30	23
Purity	95.6%	96.1%	98.7%	97.9%	97.5%
wR_p	3.72%	3.43%	3.99%	3.16%	4.46%
RF^2	3.32%	2.18%	3.48%	2.28%	3.12%
Chi2	2.04	1.98	2.38	1.96	1.93
Ba1 (0.5, 0.5, *z*)	0	0	0	0	0
Ba2 (0.5, 0.5, *z*)	0.1463(1)	0.1466(1)	0.1470(1)	0.14720(8)	0.14786(8)
Sc1/In1 (0, 0, *z*)	0.0731(3)	0.0746(1)	0.0750(2)	0.0757(1)	0.0751(1)
O1 (0.5, 0, *z*)	0.0835(5)	0.0842(5)	0.0848(6)	0.0859(4)	0.0840(5)
O2 (0, 0, *z*)	0	0	0	0	0
Cu1 (0.5, 0, *z*)	0.25	0.25	0.25	0.25	0.25
S1 (0, 0, *z*)	0.2002(4)	0.2009(4)	0.2016(4)	0.2023(3)	0.2022(3)

Table S1. All structures refined in I4/mmm. Errors are 2 sigma. Fractional occupancy of the shared Sc/In sites was fixed, based on expected ratio from target composition. Atoms were modelled with fixed thermal isotropic thermal displacement ellipsoids, depending on atom type. U_{iso}: Ba 0.02 Å^2, Sc 0.005 Å^2, In 0.01 Å^2, O 0.02 Å^2, Cu 0.025 Å^2, S 0.012 Å^2.

	$Ba_3In_2O_5Cu_2S_2$*	$Ba_3In_2O_5Cu_2S_{1.5}Se_{0.5}$	$Ba_3In_2O_5Cu_2SSe$	$Ba_3In_2O_5CuS_{0.5}Se_{1.5}$	$Ba_3In_2O_5Cu_2Se_2$
Lattice parameter a	4.1862(1)	4.1958(2)	4.2060(2)	4.2138(2)	4.2225(1)
Lattice parameter c	27.444(1)	27.5758(9)	27.7161(9)	27.841(2)	27.985(1)
Cell Volume	480.95(2)	485.47(5)	490.31(5)	494.35(6)	498.94(4)
Data Points	4345	4444	4444	4148	4444
Reflections (325 phase)	98	106	108	98	111
Refined Parameters	23	30	30	28	32
Purity	97.5%	98.7%	98.6%	98.5%	97.8%
wR_p	4.46%	3.87%	4.11%	4.55%	4.28%
RF^2	3.12%	3.55%	3.85%	4.74%	3.30%
Chi2	1.93	1.72	1.93	3.50	2.19
Ba1 (0.5, 0.5, *z*)	0	0	0	0	0
Ba2 (0.5, 0.5, *z*)	0.14786(8)	0.14693(8)	0.14609(8)	0.1449(1)	0.1440(1)
In1 (0, 0, *z*)	0.0751(1)	0.0748(1)	0.0744(1)	0.0745(1)	0.0738(1)
O1 (0.5, 0, *z*)	0.0840(5)	0.0829(5)	0.0805(5)	0.0799(6)	0.0810(5)
O2 (0, 0, *z*)	0	0	0	0	0
Cu1 (0.5, 0, *z*)	0.25	0.25	0.25	0.25	0.25
S1/Se1 (0, 0, *z*)	0.2022(3)	0.2013(2)	0.2007(2)	0.2001(2)	0.1996(1)

Table S2. All structures refined in I4/mmm. Errors are 2 sigma. Fractional occupancy of the shared S/Se sites was fixed, based on expected ratio from target composition. Atoms were modelled with fixed thermal isotropic thermal displacement ellipsoids, depending on atom type. U_{iso}: Ba 0.02 Å^2, In 0.01 Å^2, O 0.02 Å^2, Cu 0.025 Å^2, S 0.012 Å^2, Se 0.012 Å^2.* This sample is the same as the end member of series 1

Material	Ch1-Cu1-Ch1 / °	Cu1-Ch1/Å / Å	Ch block height/Å	O1-Sc1/In1-O2 / °	Sc1/In1-O1/Å (eq)	Sc/In1/O2/Å (ax)	Oxide block (Ba1-Ba1) / Å
$Ba_3Sc_2O_5Cu_2S_2$	113.7(5)	2.475(6)	2.71(2)	97.8(5)	2.092(3)	1.98(1)	7.941(4)
$Ba_3Sc_{1.5}In_{0.5}O_5Cu_2S$	114.6(4)	2.471(6)	2.67(2)	97.2(4)	2.095(2)	2.029(6)	7.982(3)
$Ba_3ScInO_5Cu_2S_2$	115.3(5)	2.467(6)	2.64(2)	97.3(5)	2.101(3)	2.049(6)	8.033(4)
$Ba_3Sc_{0.5}In_{1.5}O_5Cu_2S$	115.9(4)	2.464(5)	2.61(2)	97.7(4)	2.107(2)	2.073(4)	8.067(3)
$Ba_3In_2O_5Cu_2S_2$	115.8(4)	2.471(5)	2.63(2)	96.7(4)	2.107(2)	2.062(3)	8.116(2)
$Ba_3In_2O_5Cu_2S_{1.5}Se_{0.5}$	114.8(1)	2.490(4)	2.68(1)	96.1(4)	2.110(2)	2.062(3)	8.103(3)
$Ba_3In_2O_5Cu_2SSe$	114.0(1)	2.507(3)	2.73(1)	94.6(4)	2.110(1)	2.062(3)	8.098(3)
$Ba_3In_2O_5Cu\ S_{0.5}Se_{1.5}$	113.2(2)	2.524(3)	2.78(1)	94.1(5)	2.112(1)	2.074(3)	8.069(3)
$Ba_3In_2O_5Cu_2Se_2$	112.5(1)	2.540(2)	2.82(1)	95.4(4)	2.121(2)	2.067(3)	8.057(3)

Table S3. Selected bond distances and angles derived from Rietveld refinement to X-ray powder diffraction patterns. Also included are the heights of the chalcogenide and oxide blocks. Errors are two sigma. $Ba_3In_2O_5Cu_2S_2$ is shared by both solid solutions

Table S4: The cell lattice parameters, atomic distances and angles calculated for each end member using the HSE06 hybrid functional.

HSE06	$[Cu_2S_2][Ba_3Sc_2O_5]$	$[Cu_2S_2][Ba_3In_2O_5]$	$[Cu_2Se_2][Ba_3In_2O_5]$
a=b (Å)	4.15	4.19	4.22
c (Å)	27.38	27.73	28.03
α,β,ɣ (°)	90	90	90
Vol. ($Å^{3)}$	471.48	487.91	499.67
Cu-Ch (Å)	2.45	2.46	2.53
Cu-Cu (Å)	2.93	2.97	2.99
∠Cu-Ch-Cu (°)	115.68	117.09	113.01
Ba-O (Å)	2.93,2.70,3.08	2.71,2.97,3.17	2.70,2.99,3.16
M-O (Å)	2.09,1.99	2.08,2.12	2.07,2.13
Ba-Ba (Å) (inter layer)	8	8.2	8.08

Table S5: The cell lattice parameters, atomic distances and angles calculated for each end member using the PBEsol functional.

PBEsol	$[Cu_2S_2][Ba_3Sc_2O_5]$	$[Cu_2S_2][Ba_3In_2O_5]$	$[Cu_2Se_2][Ba_3In_2O_5]$
a=b (Å)	4.12	4.18	4.22
c (Å)	26.91	27.16	27.69
α,β,ɣ (°)	90	90	90
Vol. ($Å^{3)}$	457.66	475.44	494.12
Cu-Ch (Å)	2.41	2.42	2.51
Cu-Cu (Å)	2.92	2.96	2.99
∠Cu-Ch-Cu (°)	117.50	119.50	114.78
A-O (Å)	2.68,2.92,06	2.69,2.96,3.16	2.7,2.99,3.16
M-O (Å)	1.98,2.08	2.08,2.11	2.07,2.13
A-A (Å)	7.94	8.13	8.05

Table S6: The percentage states at the valence band maxima (VBM) and conduction band minima (CBM) for each end member.

		Cu: s,p,d /%	***Ch*: s,p,d /%**	**A^{2+}: s,p,d /%**	**M^{3+}: s,p,d /%**	**O: s,p,d /%**
$Ba_3Sc_2O_5Cu_2S_2$	**VBM**	0,2,***55***	0,***41***,0	0,1,0	0,0,0	0,1,0
	CBM	***36***,0,15	0,0,0	0,0,***45***	0,0,0	2,2,0
$Ba_3In_2O_5Cu_2S_2$	**VBM**	0,2,***55***	0,***41***,0	0,1,1	0,0,0	0,0,0
	CBM	5,0,0	6,1,0	4,0,0	***64***,2,1	***17***,0,0
$Ba_3In_2O_5Cu_2Se_2$	**VBM**	0,2,***48***	0,***47***,0	0,1,1	0,0,0	0,1,0
	CBM	5,0,1	7,0,0	3,0,0	***63***,3,1	***17***,0,0

Table S7: The calculated HSE06 effective masses for each end member.

	(light,heavy)	$[Cu_2S_2][Ba_3Sc_2O_5]$	$[Cu_2S_2][Ba_3In_2O_5]$	$[Cu_2Se_2][Ba_3In_2O_5]$
	Γ -X /m_e	~42, ~61	~84, ~210	~41, ~51
VBM	**Γ -N /m_e**	0.44, 1.96	0.38, 1.96	0.26, 1.7
	Γ -Z /m_e	0.65, 0.76	0.51, 0.81	0.37, 0.56
	X- Γ /m_e	0.95	-	-
CBM	**Γ -X /m_e**	-	0.21	0.18
	Γ -N /m_e	-	0.21	0.19
	Γ -Z /m_e	-	0.21	0.19

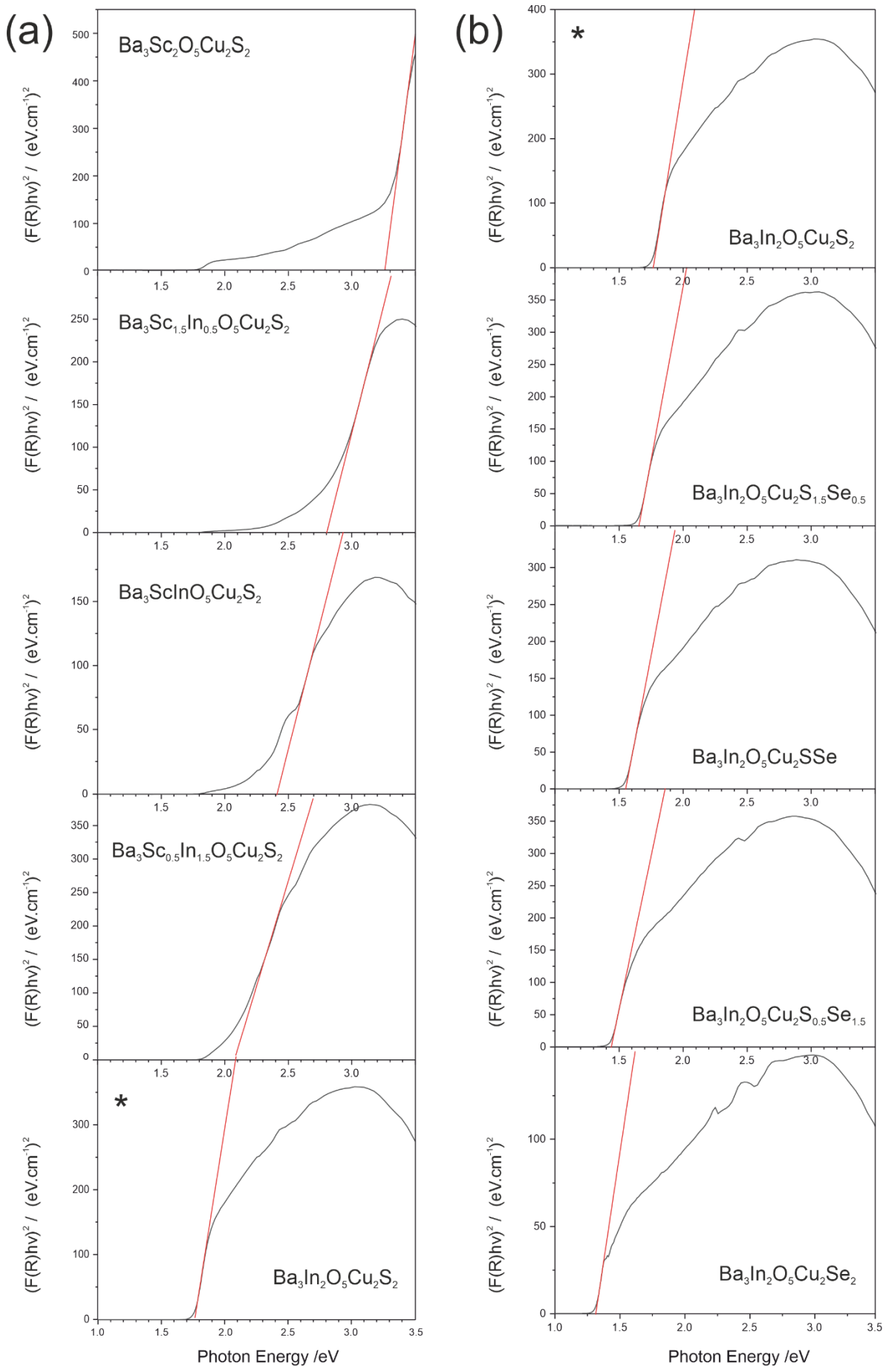

Figure S4. Tauc plots for each of the samples in the two solid solutions, (a) $Ba_3(Sc,In)_2O_5Cu_2S_2$ and (b) $Ba_3ScIn_2O_5Cu_2(S,Se)_2$ derived from diffuse reflectance spectroscopy. In each plot the red line shows the tangent used to determine the band gap of the sample. *This sample is shared by both series, data repeated.

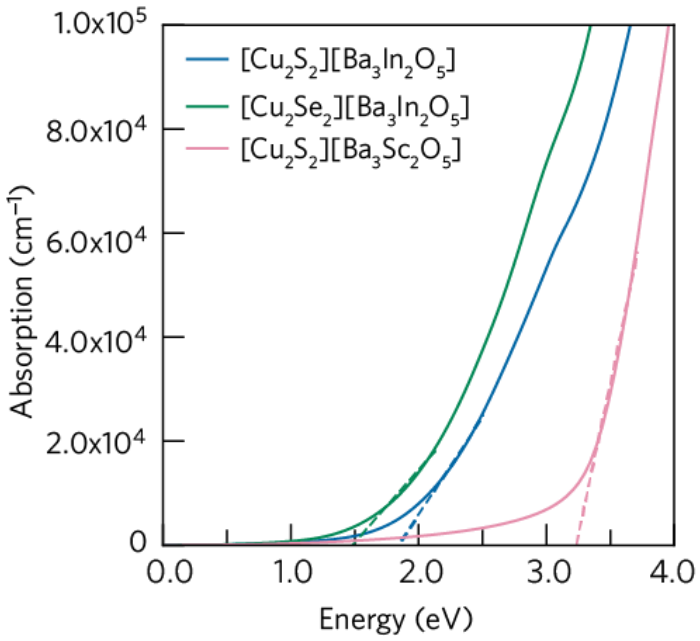

Figure S5 : The calculated optical absorption spectrum for each end member compound. A linear regression for the strong absorption onset is given by the dashed lines.

The phonon dispersion curves are given for the compounds $[Cu_2S_2][Ba_3Sc_2O_5]$, $[Cu_2S_2][Ba_3In_2O_5]$, and $[Cu_2Se_2][Ba_3In_2O_5]$ in **Figure S6a-c** respectively. Each compound is dynamically stable as there are no negative frequencies at the Γ point. In $[Cu_2S_2][Ba_3In_2O_5]$, and $[Cu_2Se_2][Ba_3In_2O_5]$ however, imaginary frequencies arise at the N and Z points in the 1st Brillouin zone indicating a potential instability in those directions. It is important to note, however, that it is possible mode-melting will be arise towards RTP due to an increased anharmonic stabilisation as well as thermal expansion, thus, whilst the *I4/mmm* structure may not be the 0K ground state structure, it will exist at RTP as affirmed by the experimental synthesis of each end member compound. The parent compound on which these compounds are based, $[Cu_2S_2][Sr_3Sc_2O_5]$, itself displays imaginary frequencies away from the Γ point.

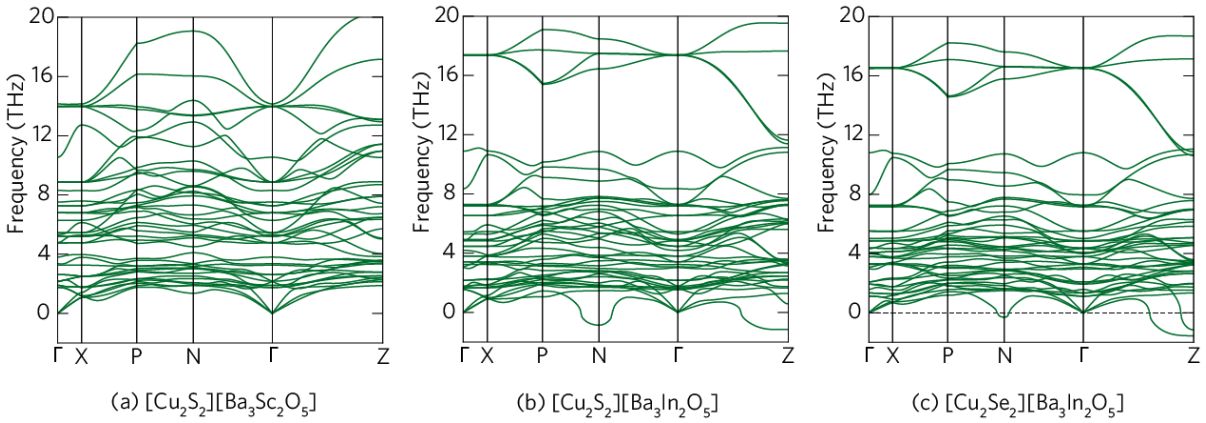

Figure S6 : The phonon dispersion spectra for each end member compound. Each spectrum is plotted from -2 to 20 THZ and shows that each compound is dynamically stable at Γ.

From the phonon dispersion curves given in SI Figure S6, the phonon bands that intersect with the Γ-point can be analysed for their IR or Raman activity. It was found that A_{2u} and E_u modes existed that are IR active between 0 and 800 cm^{-1}. FTIR data were collected in the range 400-1000 cm^{-1}, unfortunately data below 400 cm^{-1} could not be recorded due to the cut off window of the spectrometer. The calculated and recorded spectra are given in Figure S7 and the peak positions are tabulated in Table S8 alongside their respective symmetries. It is known from previous DFT studies using the PBEsol functional that peak positions can be shifted systematically by ~-10-11 cm^{-1} due to the differences in lattice parameters calculated at the athermal limit to that from experiment at finite temperatures.[1,2] We observe a relative good match for the position of the E_u absorption between the modelled and recorded data, with the model underestimating position of the A2u by 20-30 cm^{-1}, although trend in shift is replicated. In figure S8 the position of the A2u and Eu absorption for all of the members of the two solid solutions are shown, alongside the modelled values of the end members.

Symmetry of IR peak	E_u	A_{2u}	E_u	A_{2u}	E_u	A_{2u}	E_u	A_{2u}	E_u	A_{2u}	E_u	A_{2u}
$Ba_3Sc_2O_5Cu_2S_2$ (model)	63	72	87	127	159	160	173	178	296	352	467	711
$Ba_3Sc_2O_5Cu_2S_2$ (measured)	Outside of spectrometer range										481	736
$Ba_3In_2O_5Cu_2S_2$ (model)	56	72	103	114	140	149	161	164	240	279	579	670
$Ba_3In_2O_5Cu_2S_2$ (measured)											566	693
$Ba_3In_2O_5Cu_2Se_2$ (model)	44	53	70	102	110	133	135	144	239	266	551	675
$Ba_3In_2O_5Cu_2Se_2$ (measured)											543	703

Table S8. The tabulated peak positions for the calculated IR Spectroscopy for each compound together with the associated symmetry

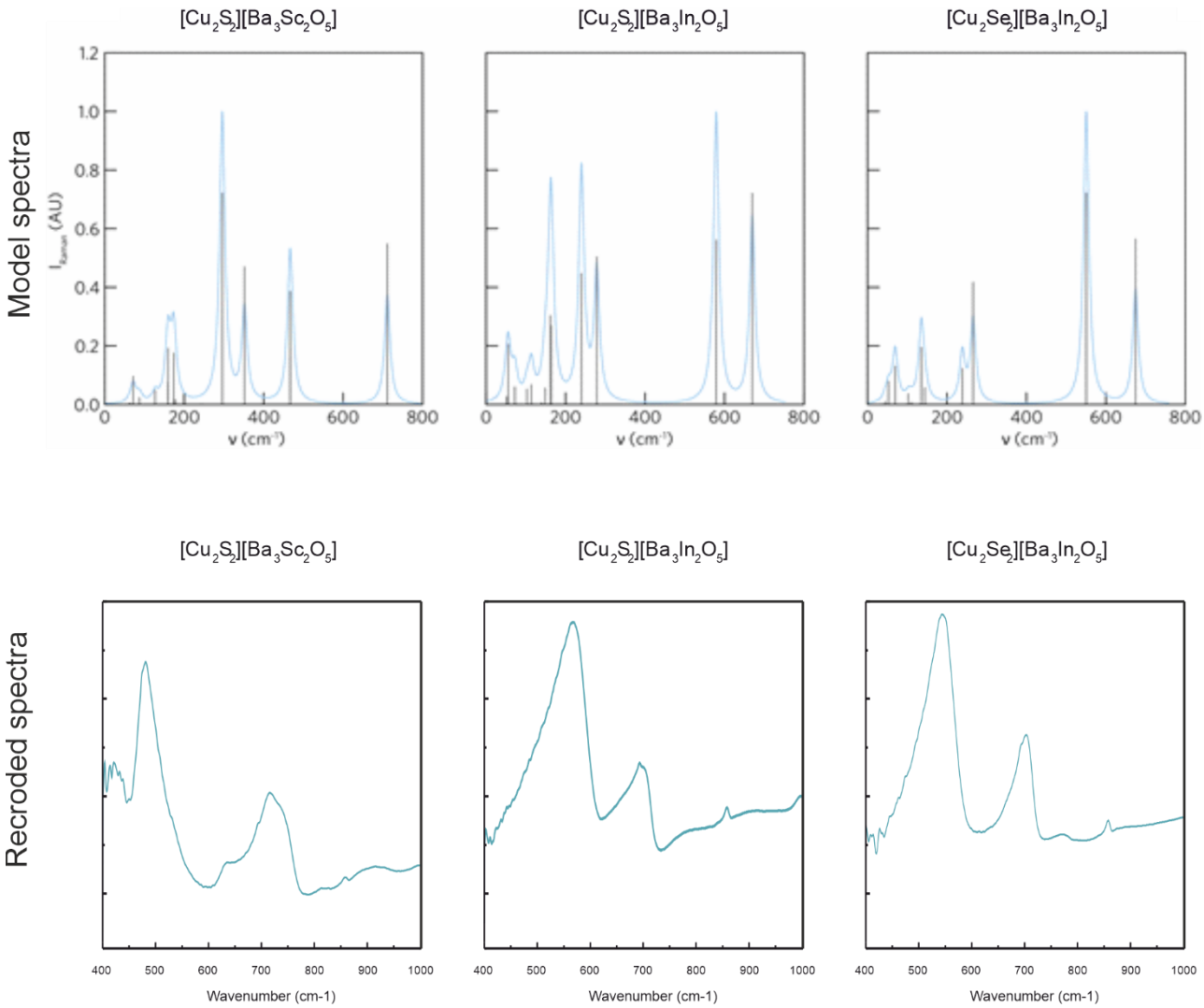

Figure S7. Model and recorded IR spectra for $Ba_3Sc_2O_5Cu_2S_2$, $Ba_3In_2O_5Cu_2S_2$ and $Ba_3In_2O_5Cu_2Se_2$

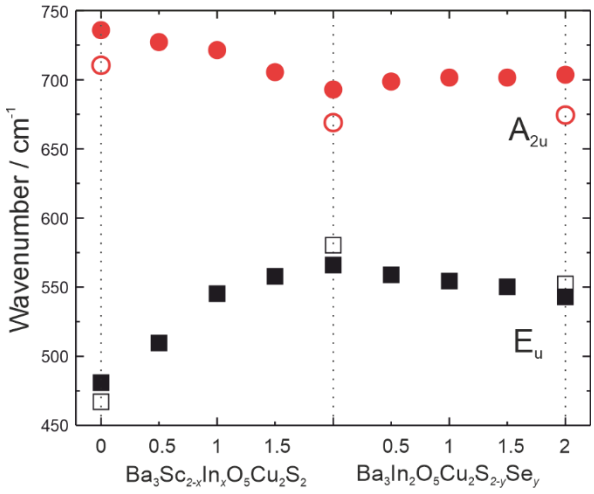

Figure S8. Plot of the position of the A2u (red circle) and Eu peaks (black square) found above 400 cm^{-1} for both solid solutions, and the predicted positions (open symbols) of the end members from computational modelling.

References:

1. Fleck, N. et al. Identifying Raman modes of Sb2Se3 and their symmetries using angle-resolved polarised Raman spectra. J. Mater. Chem. A 8, 8337–8344 (2020).

2. Whittles, T. J. et al. Band Alignments, Band Gap, Core Levels, and Valence Band States in Cu3BiS3 for Photovoltaics. ACS Appl. Mater. Interfaces 11, 27033–27047 (2019).